Fusion Engineering and Design 220 (2025) 115368

Contents lists available at ScienceDirect

Fusion Engineering and Design

journal homepage: www.elsevier.com/locate/fusengdes

Thermal-hydraulic analysis of the CORC® conductor for the DEMO CS coil

Monika Lewandowska [a,b,*], Aleksandra Dembkowska [a,b], Rafał Ortwein [a], Arend Nijhuis [c], Giulio Anniballi [c], Lorenzo Giannini [d], Danko C. van der Laan [e], Jeremy Weiss [e], Gianluca De Marzi [f], Davide Uglietti [g]

[a] The Henryk Niewodniczański Institute of Nuclear Physics, Polish Academy of Sciences 31-342 Krakow, Poland
[b] West Pomeranian University of Technology, Szczecin, 70-310 Szczecin, Poland
[c] University of Twente, Faculty of Science and Technology, Enschede, the Netherlands
[d] DEMO Central Team (DCT), EUROfusion, Garching, Germany
[e] Advanced Conductor Technologies (ACT) & the University of Colorado, Boulder, CO, USA
[f] Nuclear Department, ENEA, Frascati Research Center, Frascati 00044, Italy
[g] Ecole Polytechnique Federale Lausanne (EPFL), Swiss Plasma Center (SPC) CH-8049 Villigen PSI, Switzerland

ARTICLE INFO

Keywords:
EU DEMO
CS coil
thermal-hydraulic analysis
temperature margin
CORC® conductor

ABSTRACT

Conductors using High Temperature Superconductor (HTS) tapes are considered as a very promising solution for future high-field fusion magnets. Various HTS cable concepts, such as e.g. twisted stack cable, cross-conductor (CroCo), Roebel assembled coated conductor (RACC), conductor on round core (CORC®), HTS cable-in-conduit conductor (CICC), aligned stacks transposed in Roebel arrangement (ASTRA) have been proposed. Some of them are already considered for potential use in some components of the EU-DEMO magnet system. Recently a design of a conductor based on the CORC® concept for the innermost layer of the hybrid Central Solenoid (CS) coil of EU-DEMO was proposed. In the present work we simulated, using the THEA code by Cryosoft, normal operation of this conductor during the current cycle. Two variants of the CS1 geometry were considered: a single CS1 module, and a CS1 module split into two sub-modules (CS1L and CS1U) located one above the other. Taking into account heat loads due to the hysteresis and coupling losses, resulting from time evolution of the magnetic field profile along the conductor, we estimated the minimum temperature margin in the conductor, to verify if it fulfills the performance criterion: $\min(\Delta T_{marg}) > 1.5$ K. The results obtained with the 1D THEA model were complemented by the results of simulations with the ANSYS Mechanical APDL model (3D solid + 1D fluid) aimed at the assessment of radial temperature gradients in the conductor cross-section.

1. Introduction

The EUROfusion consortium is designing the European Demonstration Fusion Power (EU-DEMO) plant, a tokamak-based reactor capable of producing several hundred megawatts of net electricity. EU-DEMO serves as a crucial stepping stone between the ITER experimental reactor and future commercial fusion power plants [1–4]. Its fully superconducting magnet system comprises toroidal field (TF) coils, a central solenoid (CS), and outer poloidal field (PF) coils, which are being designed and assessed by the EUROfusion Work Package Magnets (WPMAG) team [5–8].

High Temperature Superconductors (HTS) offer a highly promising solution for future high-field fusion magnets due to their significantly superior performance, in particular much higher upper critical magnetic field and critical temperature, compared to Low Temperature Superconductors (LTS) [9–11]. Numerous HTS cable concepts have been proposed, including: twisted stacked-tape cable [12], cross-conductor (CroCo) [13], Roebel assembled coated conductor (RACC) [14], conductor on round core (CORC®) [15–18], HTS cable-in-conduit conductor (CICC) [19], aligned stacks transposed in Roebel arrangement (ASTRA) cable [20], vacuum pressure impregnated, insulated, partially transposed, extruded, and roll-formed (VIPER) cable [21], etc. Several of these concepts are already under consideration for potential integration into the EU-DEMO magnet system, e.g. in the inner layers of the CS coil [22–24] or in the TF coil [25–28].

Recently a design of a conductor based on the CORC® concept for the EU-DEMO CS coil was proposed. In the present work we studied its thermal-hydraulic performance in normal operating conditions by

* Corresponding author.
E-mail address: monika.lewandowska@ifj.edu.pl (M. Lewandowska).

https://doi.org/10.1016/j.fusengdes.2025.115368
Received 6 December 2024; Received in revised form 7 June 2025; Accepted 23 July 2025
Available online 1 August 2025

Table 1
Characteristics of the DEMO CS conductor relevant for the present analysis.

Description (Unit)	Value
Max. nominal magnetic field (T)	18
Conductor length, *L* (m)	736.9
Helium channel diameter (mm)	8.74
Central channel cross-section (mm^2)	59.96
Cu profile and keystones cross-section (mm^2)	490.3
Jacket cross-section (mm^2)	780.4
Single CORC® strand	
REBCO cross-section (mm^2)	0.370
Copper in tapes cross-section (mm^2)	2.057
Copper in the strand core cross-section (mm^2)	22.90
Hastelloy cross-section (mm^2)	10.29
Silver cross-section (mm^2)	0.782

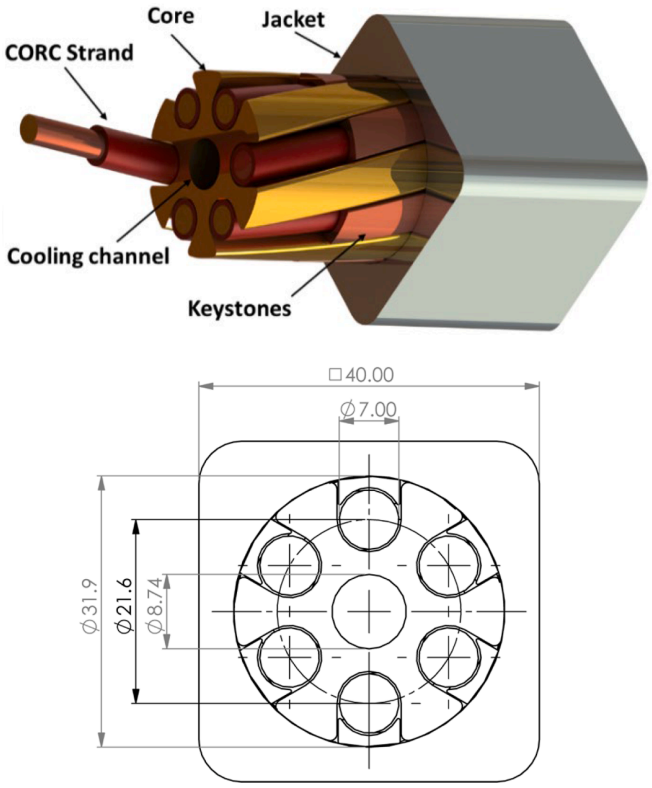

Fig. 1. Schematic layout of the CORC® conductor [17].

numerical simulations using the THEA code by CryoSoft (1D model). The goal of this work is estimation of the minimum temperature margin (ΔT_{marg}), defined as:

$$\Delta T_{marg}(x,\ t)\ =\ T_{cs}(x,\ t)\ -\ T_{sc}(x,\ t), \tag{1}$$

where T_{cs} is the current sharing temperature and T_{sc} is the superconductor operating temperature, and verification if it fulfills the min $\Delta T_{marg} > 1.5$ K acceptance criterion [5–8]. In addition, we developed the ANSYS APDL model (3D solid + 1D fluid) of a short piece of the considered conductor, to check how large transverse temperature gradients can be expected in different conductor components, and thus to verify if the use of 1D THEA model in thermal-hydraulic simulations can be justified.

Table 2
Characteristic points of the DEMO CS1 current cycle shown in Fig. 2.

Point	t (s)	I (A)
Start of current cycle	0	0
End of *Premag*	500	65,000
SOF	600	−10,716
EOF	7810	−65,000
EOP	7910	0
End of current cycle	8010	0

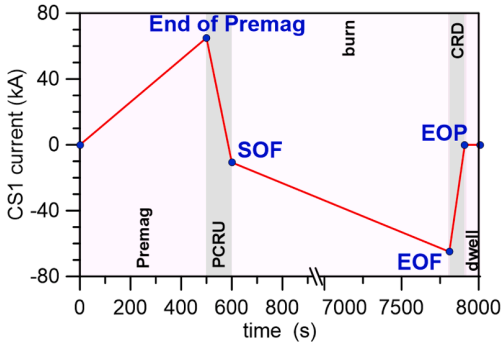

Fig. 2. Assumed DEMO CS1 current scenario.

2. The CORC® concept for the innermost layer of the DEMO CS coil

The EU-DEMO tokamak's superconducting CS will consist of five vertically stacked modules: CSU3, CSU2, CS1, CSL2, and CSL3. The central CS1 module will experience the most demanding conditions, including the highest mechanical stress and magnetic field. The expected maximum value of magnetic field in the innermost layer of the CS1 module can be as high as 18 T, which excludes the use of LTS. A design of a 65 kA HTS conductor based on the CORC® concept was developed by the ACT team [17]. The University of Twente team proposed this conductor layout for the innermost layer of the hybrid CS1 module of the EU-DEMO. The considered conductor consists of 6 twisted CORC® strands embedded in a copper profile with a central cooling channel. The copper profile and keystones constitute the distributed CORC® strands support structures. Twist pitch of the CORC® strands is 0.385 m. Each strand contains 12 layers of SuperPower HTS tapes with three tapes per layer. Relevant conductor characteristics are listed in Table 1, while the schematic layout of the conductor design is shown in Fig. 1.

3. Model assumptions

3.1. Current scenario

We assumed the following simplified plasma scenario [24,29], which includes:

500 s - premagnetisation phase (Premag),

100 s - plasma current ramp-up (PCRU) phase,

7210 s - burn phase (between the Start of Flat Top (SOF) and the End of Flat Top (EOF)),

100 s - conductor current ramp down (CRD) phase (between the EOF and End of Plasma (EOP)),

100 s - dwell phase between the EOP and start of next Premag.

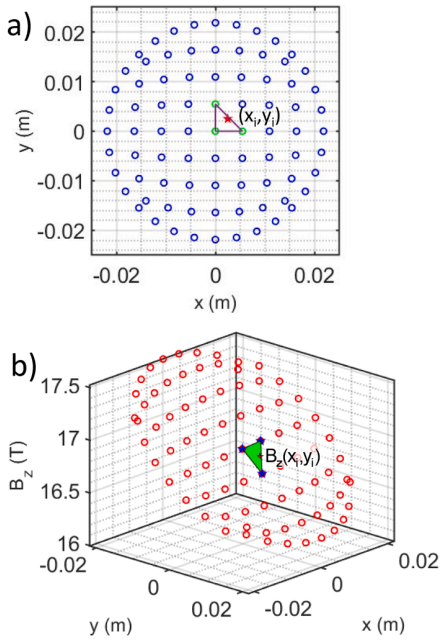

Fig. 3. (a) Distribution of nodes in which the MF components were calculated, within the cable cross-section and (b) typical values of the vertical MF component in the cable cross-section at the end of Premag.

Table 2 presents the conductor operating currents at characteristic points of the cycle. The ratio of $I_{End\ of\ Premag}$: I_{SOF}: I_{EOF} is equal to the respective proportion of total currents in the CS1 module of the DEMO 2018 reference design 58.23 MAt: - 9.6 MAt: - 58.23 MAt [29]. Currents between the characteristic points (End of Premag, SOF, EOF and EOP) were calculated through linear interpolation. This current scenario, depicted in Fig. 2, is significantly more thermally demanding than those used in thermal – hydraulic analyses of EU-DEMO of some earlier CS coil designs [30–33]. This is primarily due to the presence of two consecutive phases with substantial heat loads: Premag and PCRU.

3.2. Scaling law

Since the parameters of scaling law for the considered CORC® conductor are not available yet, we decided to use the scaling law in the following form [12]:

$$I_c(B,T) = \frac{A}{B}\left(\frac{B_{irr}(T)}{B_{irr0}}\right)^{\beta}\left(\frac{B}{B_{irr}(T)}\right)^{p}\left(1-\frac{B}{B_{irr}(T)}\right)^{q} \tag{2a}$$

$$B_{irr}(T) = B_{irr0}\left(1-\frac{T}{T_c}\right)^{\alpha} \tag{2b}$$

where $B_{irr0} = 120$ T and $T_c = 92.83$ K are the irreversible field and critical temperature, respectively. The values of $\alpha = 1.7059$, $\beta = 1.8250$, $p = 0.4786$, $q = 2.5149$ were obtained by fitting the expression given by Eqs. (2) to the experimental data for the SuperPower tapes taken from [34]. The value of parameter C in Eq. (2a) was estimated to be $C = 29,462$ A/T, assuming that the maximum operating current $I_{op} = 65$ kA at $B_{max} = 18$ T and 4.5 K is equal to 80 % of I_c (i.e. I_c (B_{max}, 4.5 K) = 81.25 kA.

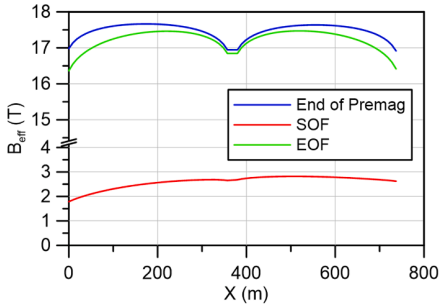

Fig. 4. Effective magnetic field profiles along the conductor (innermost layer of the CS1 module). The direction of the magnetic flux density vector at SOF and EOF is roughly opposite to that at the end of *Premag*.

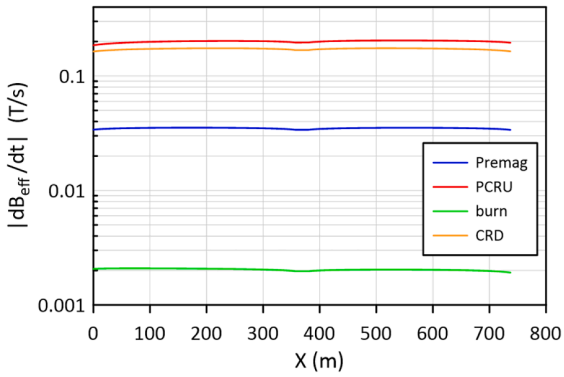

Fig. 5. Profiles of the MF time derivative in the subsequent phases of the CS1 current scenario.

3.2. Magnetic field evolution

The DCT team provided the data regarding the 3D distribution of the magnetic flux density (MF) throughout the tentative design of the CS1 module, namely: the values of $B_r(r,z)$ and $B_z(r,z)$ at 81 points spread over the conductor cross-section (see Fig. 3a), for the beginning/end of each turn of the CS1 module at characteristic points of the current cycle. Based on these results we estimated the hydraulic length of the conductor to be about 736.9 m.

The effective MF at the beginning/end of each turn of the CS1 module was obtained by solving the following equation [35]:

$$J_c\left(B_{eff\ i},T\right) = \left[\frac{1}{A_{cable}}\int\int_{A_{cable}}\left(\frac{1}{J_c(B_i(x,y),T)}\right)^{n}dxdy\right]^{-\frac{1}{n}},\ i=r,z, \tag{3}$$

where J_c is the critical current density and A_{cable} the cable cross-section. In Eq. (3) the subscripts r and z denote respectively the radial and vertical component of the magnetic field. B_{eff} was calculated for $n = 15$, which was a conservative assumption, and for $T \approx T_{op} + 1.5\ K = 6.2$ K, as suggested in [35], in order to be consistent with the design temperature margin. A dedicated procedure was developed using Matlab® to calculate the integral in Eq. (3) using 81 data points in the cable cross-section. To calculate the MF at any given point (x_i, y_i) in the cable cross-section (an example indicated as a red star in Fig. 3a), the 3 nearest nodes were found, which determined the position of the respective $B(x,y)$ plane (a green triangle in Fig. 3b). The $B(x_i, y_i)$ value was estimated from the $B(x,$

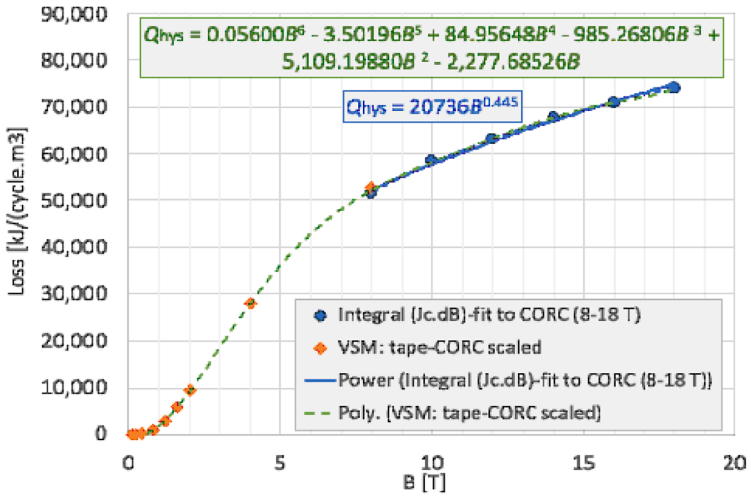

Fig. 6. The magnetization loss scaling curve with polynomial 6th order fit obtained for the applied field range of 0.1 – 18 T The power fit is valid for B in the range 8 - 18 T (and can also be used for extrapolation to 20 T). The data were normalized to the volume of superconducting tapes.

y) plane equation. The B_{eff} profile along each turn (40 turns) was obtained by linear interpolation based on the values at the beginning and end of this turn. The resulting effective magnetic field profiles along the considered conductor, at the characteristic points of the current cycle, are shown in Fig. 4.

3.3. Heat loads evolution

The coupling loss per unit length of conductor in a field ramped at a uniform rate was calculated as [36]:

$$P_{coupling}(x) = \frac{n\tau S}{\mu_0}\left(\frac{dB_{eff}(x)}{dt}\right)^2 = \frac{n\tau S}{\mu_0}\left[\left(\frac{dB_{eff\ r}(x)}{dt}\right)^2 + \left(\frac{dB_{eff\ z}(x)}{dt}\right)^2\right], \quad (4)$$

where n is the demagnetization factor, τ is the time constant dependent on the conductor parameters, and S is the superconducting tapes cross-section in strands. The values of time derivatives $\dot{B}_{eff\ r}(x)$ and $\dot{B}_{eff\ z}(x)$ during the *Premag, PCRU*, burn and *CRD* phases were estimated using the respective $B_{eff\ r}(x)$ and $B_{eff\ z}(x)$ values at the beginning and end of the given phase, e.g.

$$\left[\frac{dB_{eff_i}(x)}{dt}\right]_{PCRU} = \frac{B_{eff_i}(x)_{SOF} - B_{eff_i}(x)_{Premag}}{100\ s}, i = r, z. \quad (5)$$

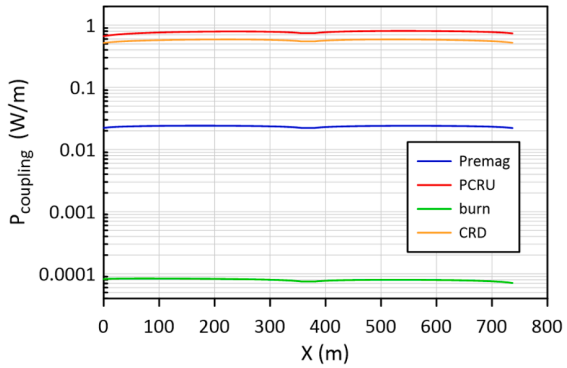

Fig. 7. Profiles of the power of coupling losses at the different phases of the current cycle for $n\tau = 300$ ms.

The resulting profiles of $|dB_{eff}/dt|$ are presented in Fig. 5.

Since the considered conductor has not yet been experimentally characterized with regard to the coupling losses, we performed the analysis for a trial value $n\tau = 300$ ms. This value was selected as a reasonable estimation based on the experimental value $n\tau = 763$ ms obtained in [37] for a single CORC® strand in a parallel MF, which can be considered as a very conservative upper limit.

The magnetization (hysteresis) loss in the conductor was computed based on the experimental fits, shown in Fig. 6, which were obtained in [38] for a similar CORC® conductor designed by ASIPP. The final version of the expression for the magnetization loss (in kJ/m^3/cycle, normalized to the HTS tapes volume) takes the form:

$$Q_{hys}(B) = \begin{cases} a_1 B^3 & \text{for } 0 < B < 0.90\ \text{T} \\ aB^6 + bB^5 + cB^4 + dB^3 + eB^2 + fB & \text{for } 0.90\ \text{T} < B < 13.37\ \text{T} \\ a_2 B^{b_2} & \text{for } 13.37\ \text{T} < B < 18\ \text{T} \end{cases}, \quad (6)$$

where $a_1 = 1953.4$, $a = 0.056$, $b = -3.50196$, $c = 84.95648$, $d = -985.26806$, $e = 5109.1988$, $f = -2277.68526$, $a_2 = 20{,}736$, $b_2 = 0.445$.

Eq. (6) estimates the thermal energy released in superconducting

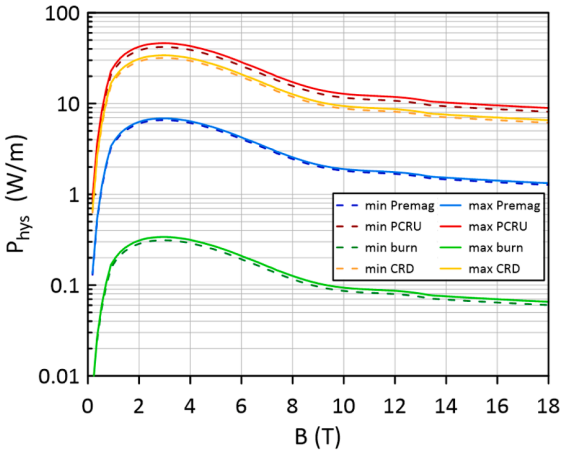

Fig. 8. Profiles of the power of hysteresis losses at the different phases of the current cycle.

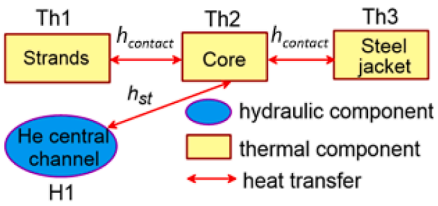

Fig. 9. Conductor components in the THEA model of the long length of conductor and thermal links between them.

tapes of a CORC® conductor subjected to periodically oscillating MF during a single period. The respective expression for the thermal power of hysteresis losses (in kW/m) is given by:

$$P_{hys}(B) = A_{tapes}\frac{dQ_{hys}}{dt} = C_{phase}A_{tapes}\left|\frac{dB}{dt}\right| \cdot \begin{cases} 3a_1B^2 & \text{for } 0 < B < 0.90 \text{ T} \\ 6aB^5 + 5bB^4 + 4cB^3 + 3dB^2 + 2eB + f & \text{for } 0.90 \text{ T} < B < 13.37 \text{ T} \\ a_2b_2B^{(b_2-1)} & \text{for } 13.37 \text{ T} < B < 18 \text{ T} \end{cases} \quad (7)$$

Each of the four linear ramps of MF occurring in the subsequent phases of the current scenario (discussed in Section 3.1) constitutes a portion of a $B(t)$ cycle with a specific frequency. Therefore, the: *Premag* (B varies from 0 to about B_{max}), *PCRU* (B varies from B_{max} down to about –0.165•B_{max}), burn (B varies from – 0.165•B_{max} down to about -B_{max}), and *CRD* (B varies from -B_{max} to 0) phases correspond to about: 0.25, 0.291, 0.209 and 0.25 cycle, respectively. Thus the factor C_{phase} in Eq. (7) is equal to 0.25, 0.291, 0.209 and 0.25 for the *Premag*, *PCRU*, burn and *CRD* phase, respectively.

The $P_{coupling}$ profiles along the conductor resulting from Eq. (4), which are constant during each phase of the current cycle and almost constant along the conductor, are presented in Fig. 7. The P_{hys} profiles along the conductor are also only slightly dependent on x but significantly vary with time during each phase, as shown in Fig. 8. It can be noticed in Figs. 7 and 8 that the *PCRU* and *CRD* phases featured the highest power of AC coupling and hysteresis losses during whole plasma cycle, due to relatively fast variations of MF. The power of coupling losses is not dominant in each phase, but it is non negligible in *PCRU* and *CRD* phases.

3.4. Cooling conditions and THEA model

The thermal – hydraulic (TH) behavior of the conductor full length operating in conditions appropriate to the innermost layer of the EU-DEMO CS1 coil was simulated using the THEA code by CryoSoft [39]. The THEA model of the conductor, shown schematically in Fig. 9, includes several 1D components connected in parallel, i.e. three solid components: the CORC® strands (thermal 1), the Cu supporting structure (Core) (thermal 2) and the jacket (thermal 3), as well as one fluid component – helium in the central cooling channel (hydraulic 1).

Heat transfer between the solid conductor components was modelled by the matrix of thermal contact resistances defined as:

$$R = 1/(h_{contact} \cdot P_{contact}), \quad (8)$$

where $P_{contact}$ is the contact perimeter and $h_{contact}$ denotes the contact conductance heat transfer coefficient. Following the common approach adopted within the EUROfusion WPMAG project team [40,41] and previous TH analyses of other designs of the EU-DEMO CS1 coil (e.g. [24,30–33,42]), a conservative value $h_{contact}$ = 500 W/(m^{2}K) was assumed [43,44]. The convective heat transfer coefficient (h_{st}) between the helium flow and the internal wall of the cooling channel was estimated using the standard smooth tube correlations, i.e. Dittus-Boelter correlation for turbulent flow and Nu_{lam} = 4.01 for laminar flow (Re < 2000) [45].

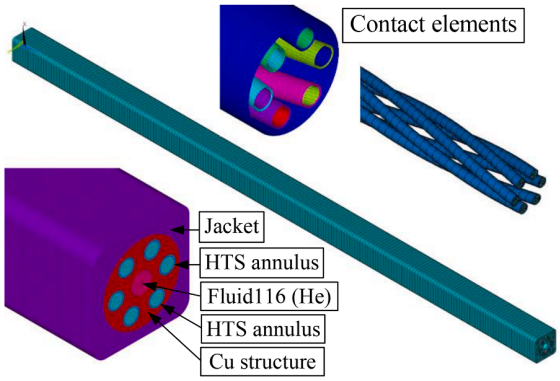

Fig. 10. Details of the mesh in the ANSYS APDL model.

The helium pressure drop in the cooling channel was estimated using friction factor correlations for smooth circular ducts [45], namely for turbulent flow, the friction factor was calculated with the Bhatti-Shah correlation:

$$f(Re) = 0.00128 + 0.1143 \cdot \mathrm{Re}^{-0.311}, \quad (12a)$$

while for laminar flow, Eq. (12b) was applied:

$$f(Re) = 16/Re. \quad (12b)$$

Adiabatic boundary conditions were applied to both ends of the solid components, while the fixed pressure (infinite reservoir) boundary conditions with the inlet pressure p_{in} = 0.6 MPa, inlet temperature T_{in} = 4.5 K and outlet pressure of 0.5 MPa were assumed for helium. These assumptions were consistent with the recommendations in [40] and with previous studies of the DEMO CS1 coil [24,30–33,42].

3.5. ANSYS APDL model of a conductor short piece

The THEA code is widely accepted as a reliable tool for TH analyses of LTS conductors. However, the considered HTS CORC® conductor has significantly different geometric properties compared to typical LTS conductors, including: (i) six CORC® macrostrands vs. about 1000 thin strands in LTS, (ii) a bulk copper structure supporting strands, and (iii) no direct contact between the CORC® strands and helium. Therefore, it is crucial to estimate the magnitude of transverse temperature gradients within the conductor cross-section to assess the validity of using a 1D model for TH analyses of this type of conductor. This was the goal of this part of our study.

We developed a parametric thermal model starting from scratch in the ANSYS Mechanical APDL software, including 3D mesh of the solid parts and 1D mesh of the fluid inside. To increase the simulation speed, a short piece of conductor of the length L = 1 m was considered.

We started to create the conductor thermal model with the simplest possible case, i.e. a uniformly heated circular pipe made either of copper or steel and cooled by helium flow. Then, subsequent components and materials were added step by step to the considered solid object, until it reproduced the actual conductor geometry. The final mature model included the following components: steel jacket, copper supporting structure, 6 twisted CORC® strands consisting of the copper core and the annular layer of HTS tapes (see Fig. 10). The solid part was meshed with SOLID278 elements, fluid with FLUID116 and the thermal contacts with CONTA174 and TARGE170. The heat source was imposed to the annular HTS region of the strands. Different constant values of the heat source power (up to 30 W/m) and contact thermal resistance between different conductor components were considered. At each stage transverse temperature gradients within the solid part were studied and a comparison with the respective THEA model was done.

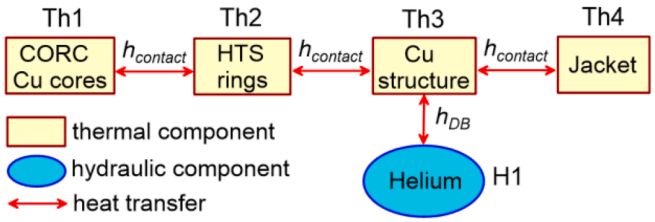

Fig. 11. Conductor components in the THEA model of the short piece of conductor and thermal links between them.

For the 1D fluid component we assumed helium flow at $p_{in} = 0.6$ MPa and $T_{in} = 4.5$ K and constant mass flow rate $\dot{m} = 9.2$ g/s, which was the expected mass flow rate in the innermost layer of the DEMO CS1 module wound with the considered CORC® conductor at no heat load. We took into account temperature dependent thermo-physical properties of helium and we assumed the standard Dittus – Boelter (h_{DB}) correlation for the convective heat transfer coefficient.

In the corresponding THEA model (shown in Fig. 11) of a short piece of conductor ($L = 1$ m), it was not possible to set a constant mass flow rate. Therefore, we applied infinite reservoir boundary conditions at both ends of the conductor. Using the Bhatti-Shah friction factor correlation (Eq. (12a)) we selected the appropriate outlet pressure to achieve a mass flow rate of about 9.2 g/s under no heat load conditions. For high powers of the thermal load imposed to the HTS rings we observed a noticeable mass flow rate reduction in the THEA model for simulation times exceeding about 20 s, leading to inconsistency between the ANSYS and THEA models. Thus, in all considered cases the simulation time was limited to the value for which the mass flow rate in the THEA model was still almost constant.

4. Results and discussion

4.1. Typical results obtained with the ANSYS APDL model of the conductor short piece

In order to observe possibly high transverse temperature gradients within the conductor cross-section we considered the heat source power possibly close to its maximum value expected during the current cycle and very conservative values of the uncertain model parameter ($h_{contact}$). Typical simulation results are presented in Fig. 12 and in Table 3. For comparison we added in Table 3 also the respective results obtained with the THEA model (shown in Fig. 11).

It is seen in Figs. 12 and in Table 3 that, despite the conservative assumptions regarding the AC losses heat source power and contact thermal resistances, the transverse temperature gradients in all conductor components observed in the ANSYS model were relatively small. The results obtained with the ANSYS and THEA models were in reasonably good agreement (the differences between the respective temperatures predicted by the ANSYS and THEA models did not exceed few tens of mK). This is an encouraging result indicating that the use of 1D models in thermal hydraulic simulations of CORC® based conductors may be justified. It is also seen in Figs. 12bc and in Table 3, that the temperature of the CORC® copper cores and HTS annular regions is very similar. This justifies lumping together these two cables components into one thermal component in the THEA model of the full conductor (shown in Fig. 9) which allows for the model simplification and shortening of the simulations time.

4.2. Results of THEA simulations of the thermal-hydraulic behavior of the innermost layer of the CS1 coil during at operation conditions

We considered two possible configurations of the CS1 geometry: the single CS1 module and the CS1 module split into two submodules (CS1L and CS1U) located one above the other. In the latter case the hydraulic length of the conductor in one sub-module was twice shorter (368.46 m) and we used in its analysis the MF and heat loads profiles corresponding to the CS1L module (left half of the full length CS1 conductor).

The analysis began with preliminary simulations of steady state with no heat load and with the current and the MF set equal to zero, i.e. conditions corresponding to the state before the start of the current cycles. These simulations started from the constant initial conditions $T(x) = T_{in}$, $p(x) = p_{in}$ and were carried out until a steady state was observed, which typically took around 1500 s. The stationary solids temperature and also helium pressure, temperature, and mass flow rate profiles along the conductor were recorded and then applied as the initial conditions for the simulations of normal conductor operation during the first full cycle of plasma operation. The mass flow rate at no heat load is typically the maximum mass flow rate observed under normal operation. The results of this steady state analysis, compiled in Table 4, agreed very well with the respective predictions of the simplified model, described in detail in [46]. Two cases mentioned above were considered: single CS1 module ("Full length" in Table 4) and CS1 module divided into two submodules CS1L and CS1U ("Half length" in Table 4). It is seen that in case of the single CS1 module the helium residence time is longer than the total duration of the dwell and *Premag* phases, which indicates some problems with conductor re-cooling after the CRD phase.

For each of cases mentioned above (single CS1 module and CS1L module) we made an attempt to simulate two plasma cycles. However, in both cases the minimum temperature margin in the conductor dropped to 0, and the conductor quenched close to the end of the first *Premag* phase (Fig. 13). The detailed simulations' results for the *Premag* phase are presented in Figs. 14a-14c and 15.

The conductor operating temperature during the *Premag* phase increases monotonically due to AC losses (Fig. 14a). The temperature rise is the fastest for times between about 40 s and 130 s when the power of hysteresis losses is the highest (above 5 W/m). Such a rapid temperature increase causes a significant pressure rise inside the conductor (Fig. 14c), resulting in substantial disturbances to the helium flow, including a flow reversal in the left portion of the cable (Fig. 15). For times $t > 130$ s, the rate of temperature increase decreases, leading to stabilization of both pressure and flow. During the whole *Premag* phase the current sharing temperature profile along the conductor phase decreases due to the rise of the operating current and MF. Both increasing strands temperature and decreasing current sharing temperature contribute to a systematic reduction in the temperature margin during the *Premag* phase (Figs. 13 and 14b).

5. Summary, conclusions and perspectives

Normal operation of the CORC® conductor designed by the ACT team for the innermost layer of the hybrid CS coil of EU-DEMO was simulated using the THEA code by CryoSoft. Simplified current scenario, which did not include the fast breakdown, was considered. Heat loads due to AC coupling losses (characterized by the value $n\tau = 300$ ms [37]) and hysteresis losses, calculated on the basis of the experimental fit obtained in [38], were taken into account. Heat loads due to hysteresis losses were estimated based on experimental fit obtained for the CORC® conductor designed by ASIPP.

In both considered cases (full conductor length – corresponding to a single CS1 module, and half conductor length – CS1 module split into two submodules CS1L and CS1U), for the assumed model of heat loads, the temperature margin was too small and the conductor quenched close to the end of the *Premag* phase. Generation of magnetization losses in the considered CORC® conductor should be studied in more details, if possible, also experimentally. It would be advisable to undertake some efforts to reduce the heat load due to magnetization losses on the cable, e.g. by reducing the tapes width or using striated tapes.

The results obtained with the respective ANSYS APDL and THEA models in the considered cases (short piece of conductor, constant

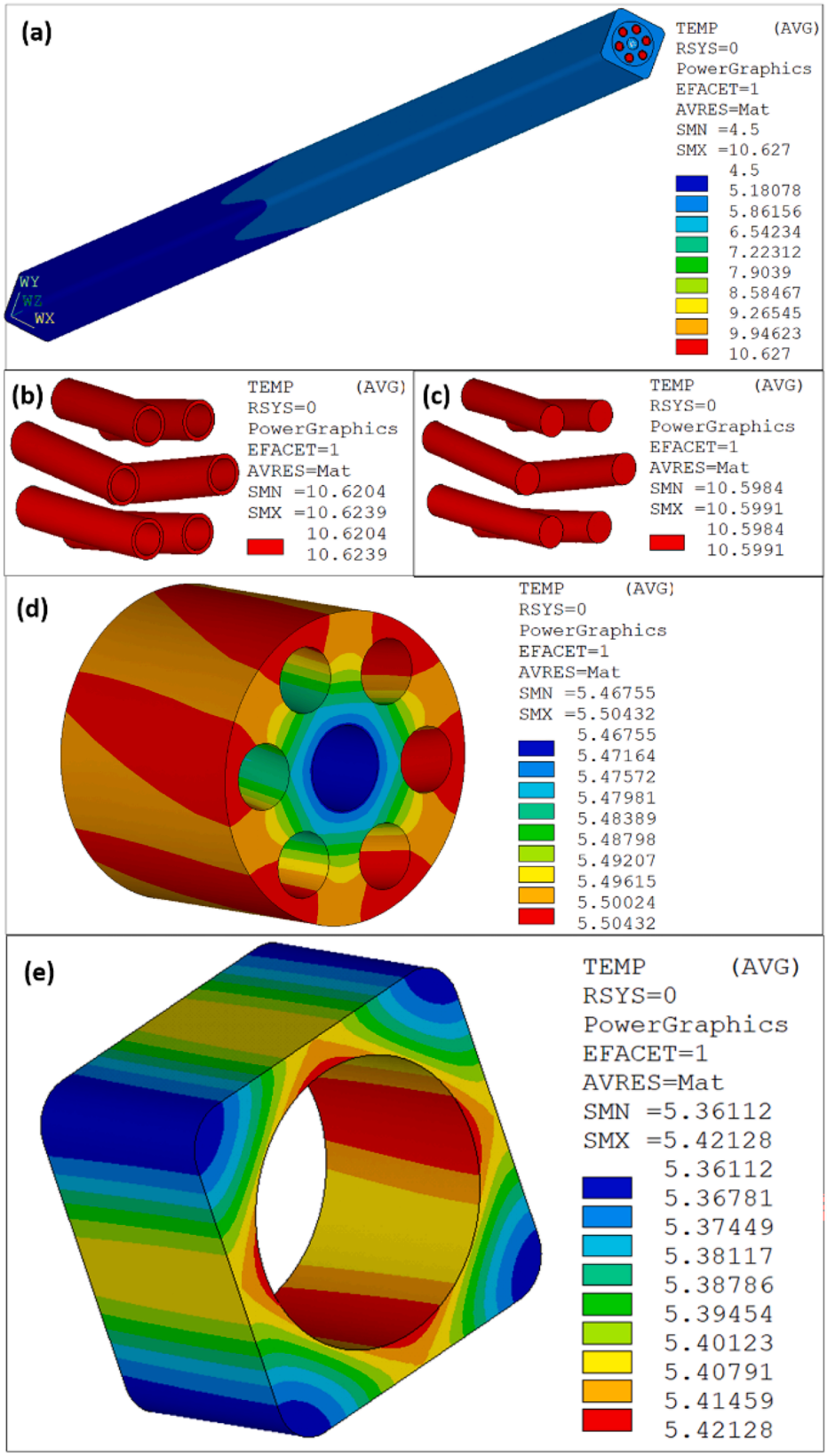

Fig. 12. Temperature distribution at $t = 18$ s in the whole considered piece of conductor (a), and in its final section ($z \approx L$) in the cross-sections of the individual cable components: HTS rings (b), copper CORC® cores (c), copper supporting structure (d), steel jacket (e). All figures (a)-(e) were obtained assuming $P = 20$ W/m = const, while the heat transfer coefficient between each pair of adjacent thermal components was assumed constant equal to $h_{contact} = 30$ W/(m^{2}K).

Table 3
Temperature of the final section of the considered short piece conductor ($z \approx L$) at $t = 18$ s, $P = 20$ W/m = const and $h_{contact} = 30$ W/(m^{2}K).

Component	Temperature (K)		
	ANSYS min	ANSYS max	THEA
Cu strand core	10.60	10.60	10.65
HTS CORC® annulus	10.62	10.62	10.68
Cu structure	5.47	5.50	5.52
Jacket	5.36	5.42	5.46
Helium	5.03		5.03

Table 4
Results of the hydraulic analysis at no heat load. Single CS1 module (full length) and CS1L module divided into two submodules CS1L and CS1U (half length) were considered.

Parameter (unit)	Full length	Half length
Mass flow rate (g/s)	9.2	13.5
Velocity (m/s)	1.1	1.6
Reynolds number (-)	$3.4 \bullet 10^5$	$5.0 \bullet 10^5$
Residence time (s)	659	225

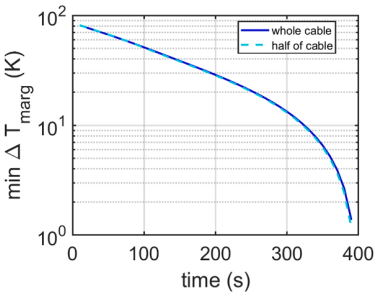

Fig. 13. Time evolution of the minimum temperature margin in the CS1 (solid line) and CS1L (dashed line) conductor.

helium mass flow rate) were in reasonably good agreement. The transverse temperature gradients in the cable cross-section observed in the ANSYS model were relatively small, despite very conservative assumptions regarding the thermal resistance between the solid conductor components. This indicates that the use of 1D models in TH simulations of the considered CORC® conductor can be justified.

Preparatory work to simulate longer length (about 50 m) of conductor (i.e. replacing the actual jacket by a cylindrical one with the same cross section, which enables considering 1/6 of the solid domain, and thus reducing significantly the simulation time) is ongoing and the preliminary results seem promising. In order to simulate longer lengths of conductor, the model of the fluid domain should also be improved to predict correctly the reduction of the mass flow rate under the influence of the heat sources.

CRediT authorship contribution statement

Monika Lewandowska: Writing – original draft, Validation, Supervision, Project administration, Investigation, Funding acquisition, Data curation, Conceptualization. **Aleksandra Dembkowska:** Writing – review & editing, Validation, Methodology, Investigation, Data curation, Conceptualization. **Rafał Ortwein:** Writing – review & editing, Investigation, Data curation, Conceptualization. **Arend Nijhuis:** Writing – review & editing, Data curation, Conceptualization. **Giulio Anniballi:** Writing – review & editing, Conceptualization. **Lorenzo Giannini:** Writing – review & editing, Investigation. **Danko C. van der Laan:** Writing – review & editing, Conceptualization. **Jeremy Weiss:** Writing – review & editing, Conceptualization. **Gianluca De Marzi:**

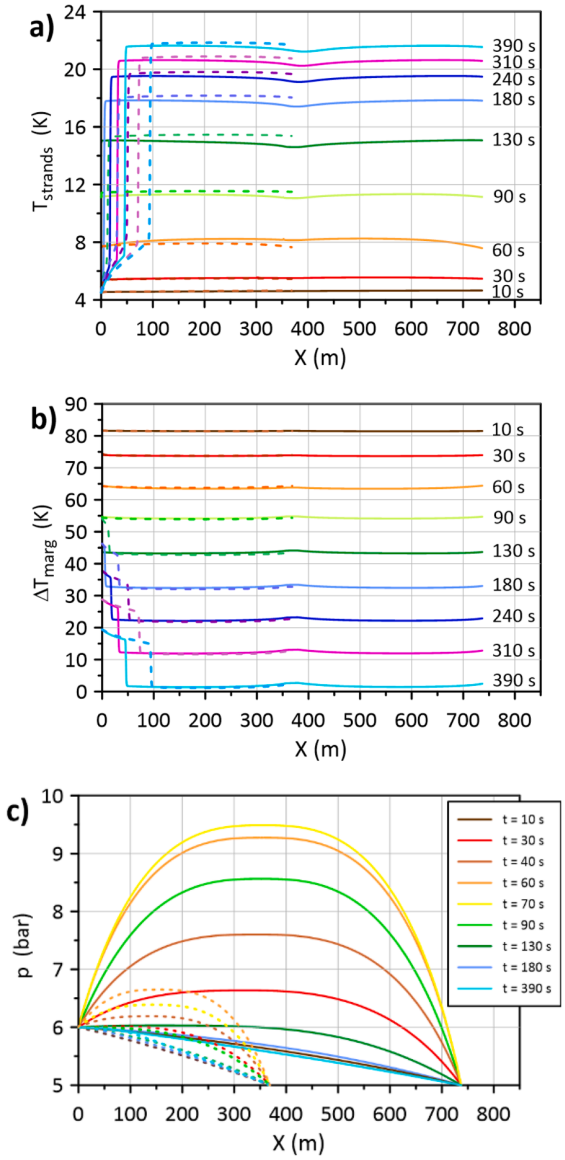

Fig. 14. Time evolution of the strands temperature (a), temperature margin (b), and pressure profiles along the CS1 (solid lines) and CS1L (dashed lines) conductors.

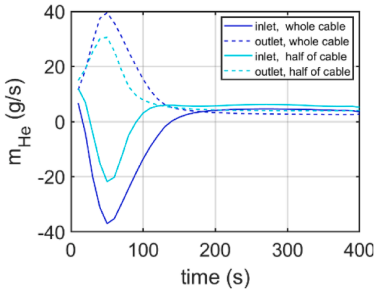

Fig. 15. Time evolution of the helium mass flow rate at the inlet and outlet of the CS1 (solid lines) and CS1L (dashed lines) conductors.

Writing – review & editing. **Davide Uglietti:** Writing – review & editing.

Declaration of competing interest

The authors declare that they have no known competing financial interests or personal relationships that could have appeared to influence the work reported in this paper.

Acknowledgments

This work has been carried out within the framework of the EUROfusion Consortium, funded by the European Union via the Euratom Research and Training Programme (Grant Agreement No 101052200 — EUROfusion). Views and opinions expressed are however those of the author(s) only and do not necessarily reflect those of the European Union or the European Commission. Neither the European Union nor the European Commission can be held responsible for them.

This work has been co-financed by the Polish Ministry of Science and Higher Education in the framework of the International Co-financed Projects (PMW) programme 5921/HEU - EURATOM/2024/2.

Part of the work has been supported by the U.S. Department of Energy under grant numbers DE-SC0014009, DE-SC0013723 and DE-SC0018125.

Research carried out on research apparatus purchased as part of the project No. RPZP.01.03.00–32–0004/18. Project co-financed by the European Union from the European Regional Development Fund under the Regional Operational Program of the West Pomeranian Voivodeship 2014–2020. Project co-financed by the Ministry of Science and Higher Education.

Data availability

Data will be made available on request.

References

[1] A.J.H. Donné, W. Morris, European research roadmap to the realisation of fusion energy, Nov. 2018, ISBN 978-3-00-061152-0.
[2] G. Federici, et al., DEMO design activity in Europe: progress and updates, Fusion Eng. Des. 136 (2018) 729–741.
[3] G. Federici, et al., Overview of the DEMO staged design approach in Europe, Nucl. Fusion 59 (2019). Art. No. 066013.
[4] G. Federici, C. Baylard, A. Beaumont, J. Holden, The plan forward for EU DEMO, Fusion Eng. Des. 173 (2021). Art. No. 112960.
[5] L. Zani, et al., Overview of progress on the EU DEMO reactor magnet system design, IEEe Trans. Appl. Supercond. 26 (4) (2016). Art. No. 4204505.
[6] V. Corato, et al., Progress in the design of the superconducting magnets for the EU DEMO, Fusion Eng. Des. 136 (2018) 1597–1604.
[7] K. Sedlak, et al., Advance in the conceptual design of the European DEMO magnet system, Supercond. Sci. Technol. (Singap. World Sci.) 33 (4) (2020). Art. No. 044013.
[8] V. Corato, et al., The DEMO magnet system – Status and future challenges, Fusion Eng. Des. 174 (2022). Art. No. 112971.
[9] W.H. Fietz, Ch. Barth, S. Drotziger, W. Goldacker, R. Heller, S.I. Schlachter, K.-P. Weiss, Prospects of high temperature superconductors for fusion magnets and power applications, Fusion Eng. Des. 88 (2013) 440–445.
[10] W.H. Fietz, M.J. Wolf, A. Preuss, R. Heller, K.-P. Weiss, High-current HTS cables: status and actual development, IEEe Trans. Appl. Supercond. 26 (2016). Art. No. 4800705.
[11] P. Bruzzone, W.H. Fietz, J.V. Minervini, M. Novikov, N. Yanagi, Y. Zhai, J. Zheng, High temperature superconductors for fusion magnets, Nucl. Fusion 58 (2018). Art. No. 103001.
[12] M. Takayasu, L. Chiesa, N.C. Allen, J.V. Minervini, Present status and recent developments of the twisted stacked-tape cable conductor, IEEe Trans. Appl. Supercond. 26 (2016) 25–34. Art No. 6400210.
[13] M.J. Wolf, C. Ebner, W.H. Fietz, R. Heller, D. Nickel, K.-P. Weiss, High temperature superconductors for fusion applications and new developments for the HTS CroCo conductor design, Fusion Eng. Des. 172 (2021). Art. No. 112739.
[14] W. Goldacker, et al., Improvement of superconducting properties in ROEBEL assembled coated conductors (RACC), IEEe Trans. Appl. Supercond. 19 (3) (2009) 3098–3101.
[15] J.D. Weiss, T. Mulder, H.J. ten Kate, D.C. van der Laan, Introduction of CORC® wires: highly flexible, round high-temperature superconducting wires for magnet and power transmission applications, Supercond. Sci. Technol. (Singap. World Sci.) 30 (2017). Art. No. 014002.
[16] D.C. van der Laan, J.D. Weiss, D.M. McRae, Status of CORC® cables and wires for use in high-field magnets and power systems a decade after their introduction, Supercond. Sci. Technol. (Singap. World Sci.) 32 (3) (2019). Art. No. 033001.
[17] J.D. Weiss, et al., Performance of low-loss demountable joints between CORC® cable-in-conduit-conductors at magnetic fields up to 8 T developed for fusion magnets, Supercond. Sci. Technol. (Singap. World Sci.) 36 (2023). Art. No. 085002.
[18] T. Mulder, J. Weiss, D. van der Laan, A. Dudarev, H. ten Kate, Recent progress in the development of CORC cable-In-conduit conductors, IEEe Trans. Appl. Supercond. 30 (4) (2020). Art No. 4800605.
[19] G. Celentano, et al., Design of an industrially feasible twisted-stack HTS cable-in-conduit conductor for fusion application, IEEe Trans. Appl. Supercond. 24 (3) (2014). Art. No. 4601805.
[20] N. Bykovskiy, H. Bajas, O. Dicuonzo, P. Bruzzone, K. Sedlak, Experimental study of stability, quench, propagation and detection methods on 15 kA sub-scale HTS fusion conductors in SULTAN, Supercond. Sci. Technol. 36 (2023) 034002, 18pp.
[21] Z.S. Hartwig, et al., VIPER: an industrially scalable high-current high-temperature superconductor cable, Supercond. Sci. Technol. 33 (2020) 11LT01, https://doi.org/10.1088/1361-6668/abb8c0, 8pp.
[22] R. Wesche, X. Sarasola, K. Sedlak, N. Bykovskiy, B. Stepanov, D. Uglietti, P. Bruzzone, DEMO central solenoid design based on the use of HTS sections at highest magnetic field, IEEe Trans. Appl. Supercond. 28 (2018). Art. No. 4203605.
[23] R. Wesche, X. Sarasola, O. Dicuonzo, I. Ivashov, K. Sedlak, D. Uglietti, P. Bruzzone, Hybrid HTS-Nb_3Sn-NbTi DEMO CS coil design optimized for maximum magnetic flux generation, Fusion Eng. Des. 146 (2019) 10–13.
[24] R. Guarino, M. Lewandowska, A. Dembkowska, N. Bykovskiy, X. Sarasola, K. Sedlak, Thermal-hydraulic analysis of alternative cable-in-conduit conductors for the European DEMO hybrid central solenoid, Fusion Eng. Des. 187 (2023). Art. No. 113368.
[25] R. Heller, P.V. Gade, W.H. Fietz, T. Vogel, K.-P. Weiss, Conceptual design improvement of a toroidal field coil for EU DEMO using high-temperature superconductors, IEEe Trans. Appl. Supercond. 26 (2016). Art. No. 4201105.
[26] W.H. Fietz, R. Heller, M.J. Wolf, P.V. Gade, High temperature superconductor cables for EU-DEMO TF-magnets, Fusion Eng. Des. 125 (2017) 290–293.
[27] M. Lewandowska, A. Dembkowska, R. Heller, M. Wolf, Thermal-hydraulic analysis of an HTS DEMO TF coil, Cryogenics 96 (2018) 125–132.
[28] M.J. Wolf, Ch. Ebner, W.H. Fietz, R. Heller, D. Nickel, K.-P. Weiss, High temperature superconductors for fusion applications and new developments for the HTS CroCo conductor design, Fusion Eng. Des. 172 (2021). Art. No. 112739.
[29] N. Ambrosino, Reference equilibrium for 2018 WPMAG DEMO single null. https://idm.euro-fusion.org/?uid=2NV5BB, 2019.
[30] R. Vallcorba, et al., Thermohydraulic analyses on CEA concept of TF and CS coils for EU-DEMO, IEEe Trans. Appl. Supercond. 28 (3) (2018). Art. No. 4202605.
[31] A. Dembkowska, M. Lewandowska, X. Sarasola, Thermal-hydraulic analysis of the DEMO CS coil, IEEe Trans. Appl. Supercond. 28 (4) (2018). Art. No. 4205605.
[32] A. Dembkowska, M. Lewandowska, X. Sarasola, Helium flow and temperature distribution in the CS1 module of the DEMO CS coil, in: Proc. 2017 International Conference on Electromagnetic Devices and Processes in Environment Protection with Seminar Applications of Superconductors (ELMECO & AoS), Lublin, 2017, pp. 1–4, https://doi.org/10.1109/ELMECO.2017.8267763.
[33] A. Dembkowska, M. Lewandowska, L. Zani, B. Lacroix, Thermal-hydraulic analysis of the DEMO CS coil designed by CEA, Fusion Eng. Des. 171 (2021). Art. No. 112557.
[34] V. Lombardo, E. Barzi, D. Turrioni, A.V. Zlobin, Critical currents of $YBa_2Cu_3O_{7-\delta}$ tapes and $Bi_2Sr_2CaCu_2O_x$ wires at different temperatures andMagnetic fields, IEEE Trans. Appl. Supercond. 21 (2011) 3247–3325.
[35] A. Torre, B. Lacroix, L. Zani, Q.Le Coz, Magn. Field Calc. Final Rep. Task (2020). MAG-2.3-T006-D001IDM reference: EFDA_D_2NH5PP.
[36] M.N. Wilson, Superconducting Magnets, Clarendon Press, 1983.
[37] K. Yagotintsev, et al., AC loss and contact resistance in REBCO CORC®, Roebel, and stacked tape cables, Supercond. Sci. Technol. (Singap World Sci.) 33 (2020). Art. No. 08500914pp.
[38] A. Nijhuis, EU-CN CORC-CICC coupling loss in transverse and parallel AC field, final report for the taskMAG-T.01.01-T026-D001 (2023), IDM reference: EFDA_D_2RD8QR.
[39] T.H.E.A. Thermal, Hydraulic and electric analysis of superconducting cables – User's guide, CryoSoft (2021). https://supermagnet.sourceforge.io/manuals/Thea_2.4.pdf.
[40] V. Corato, et al., 5Common operating values for DEMO magnets design for. http://www.euro-fusionscipub.org/archives/eurofusion/common-operating-values-for-demo-magnets-design-for-2016-2, 2016.
[41] L. Savoldi, R. Zanino, Common approach for thermal-hydraulic calculations, Memo for WPMAG-2.1-D01, https://idm.euro-fusion.org/?uid=2LMECE, 2016.
[42] A. Dembkowska, et al., Quench analysis of the DEMO CS1 coil, Cryogenics 112 (2020). Art. No. 103194.
[43] K. Takahata, H. Tamura, T. Mito, Thermal contact conductance between the bundle and the conduit in cable-in-conduit conductors, IEEe Trans. Appl. Supercond. 14 (2004) 1477–1480.
[44] N. Bagrets, R. Heller, J.R. Weis, K.-P. Weiss, Thermal resistance between metallic surfaces of copper and stainless steel at different temperatures and applied forces for high current HTS cable-in-conduit conductors, IEEe Trans. Appl. Supercond. 32 (2022). Art. No. 8800205.
[45] R.K. Shah, D.P. Sekulić, Fundamentals of Heat Exchanger Design, Wiley, New Jersey, 2003, pp. 476–483.
[46] M. Lewandowska, K. Sedlak, Thermal-hydraulic analysis of LTS cables for the DEMO TF coil, IEEe Trans. Appl. Supercond. 24 (2014). Art. No. 4200305.